Earthquake Engineering and Structural Dynamics

Experimental evaluation of ground motion scaling methods for structures with limited nonlinearity

Journal:	*Earthquake Engineering and Structural Dynamics*
Manuscript ID:	Draft
Wiley - Manuscript type:	Research Article
Date Submitted by the Author:	n/a
Complete List of Authors:	O'Donnell, Andrew; University of Notre Dame, Civil Engineering and Geological Sciences Kurama, Yahya; University of Notre Dame, Civil Engineering Kalkan, Erol; United States Geological Survey, Earthquake Science Center Taflanidis, Alexandros; University of Notre Dame, Civil Engineering and Geological Sciences Beltsar, Olga; University of Notre Dame, Civil Engineering and Geological Sciences
Keywords:	response history analysis, ground motion selection and scaling, linear-elastic structures, seismic design

SCHOLARONE™
Manuscripts

Experimental evaluation of ground motion scaling methods for structures with limited nonlinearity

A.P. O'Donnell,[1] Y.C. Kurama,[2] E. Kalkan,[3] A.A. Taflanidis,[4] O.A. Beltsar[5]

[1]*Graduate Student, Civil Engineering and Geological Sciences, Univ. of Notre Dame, 156 Fitzpatrick Hall, Notre Dame, IN 46556; PH: (617) 797-2311; email: aodonne1@nd.edu*
[2]*Professor, Civil Engineering and Geological Sciences, Univ. of Notre Dame, 156 Fitzpatrick Hall, Notre Dame, IN 46556; PH: (574) 631-8377; email: ykurama@nd.edu*
[3]*Research Structural Engineer, Earthquake Science Center, United States Geological Survey, 345 Middlefield Rd., Menlo Park, CA 94025; PH: (650) 329-5146; email: ekalkan@usgs.gov*
[4]*Rooney Family Assistant Professor, Civil Engineering and Geological Sciences, Univ. of Notre Dame, 156 Fitzpatrick Hall, Notre Dame, IN 46556; PH: (574) 631-5696; email: a.taflanidis@nd.edu*
[5]*Former Undergraduate Student, Civil Engineering and Geological Sciences, Univ. of Notre Dame, 156 Fitzpatrick Hall, Notre Dame, IN 46556; PH: (925) 353-0355; email: obeltsar@gmail.com*

SUMMARY

The task of selecting and scaling an appropriate set of ground motion records is one of the most important challenges facing practitioners in conducting response history analyses (RHA) for seismic design and risk assessment. Ironically, this is also the single task with the least guidance provided in current building codes, resulting in the use of mostly subjective choices in design. The research effort described in this paper focuses on an experimental evaluation of selected ground motion scaling methods based on extensive shake-table tests of small-scale linear-elastic building frame structures with four different fundamental periods. The experimental results are then extended to a wider range of structural periods using a validated analytical model to assess the effectiveness of the scaling methods in reducing the dispersion and increasing the accuracy in seismic demand estimates. For structures with limited nonlinearity, the test and analysis results stress the potential uncertainty from scaling methods that are based on the knowledge of the exact properties of the structure.

KEY WORDS: response history analysis; ground motion selection and scaling; linear-elastic structures; seismic design

INTRODUCTION

This paper describes an experimental investigation on the scaling of ground motion records for use in linear-elastic response history analysis (RHA) of building structures. In recent years, as performance-based seismic design considerations have become pre-requisite for controlling the level of structural and non-structural damage during an earthquake, the use of RHA has gained utmost importance. This rigorous analysis method requires, as input, a suite of ground motion records that have been selected and modified (i.e., scaled) appropriately to make them compatible with the site-specific hazard level(s) considered [e.g., Service Basis Earthquake (SBE); Design Basis Earthquake (DBE)]. Ground motion scaling has a large impact on RHA results, governing the outcome and amount of uncertainty from seismic design. Ironically, this is also the single task with the least guidance provided

For Peer Review

in current building codes and provisions, resulting in the use of mostly subjective choices in the use of ground motions.

While the seismic design of most civil engineering structures is based on significant nonlinear behavior under a large earthquake, the dynamic response of linear-elastic systems is relevant for many applications such as critical structures that are required to remain linear-elastic (e.g., nuclear power reactor buildings), very tall or very short structures, and structures under small or moderate seismic activity where significant nonlinearity is not expected (e.g., service level response). Considering these issues, this paper focuses on the measured response from small-scale shake-table experiments of linear-elastic multi-story building frame structures under ground motion sets that have been scaled using different methods. The experimental results are then extended to a wider range of structural periods using a validated analytical model to assess the effectiveness of the scaling methods in reducing the dispersion and increasing the accuracy in the lateral displacement demands.

Most of the research to date on ground motion scaling has been on single-degree-of-freedom systems [e.g., 1-11], with fewer studies on multi-degree-of-freedom systems [12-20]. For scaling methods that depend on an estimated fundamental period for the structure, no consideration has been given on the impact of errors in the estimated period. Furthermore, the previous research is based solely on numerical simulations, with no experimental data available for the validation of the results. While previous shake-table experiments of small-scale linear-elastic structures are available in the literature [e.g., 21-24], none of these studies have investigated ground motion scaling. These factors have contributed to a lack of consensus on which scaling methods would be best suited to achieve reliable, robust median demand estimates over a range of structural properties. The shake-table tests described in this paper form the first experimental study to evaluate the accuracy (that is, ability to provide accurate estimates of the median demands as if a much larger set of records were used) and efficiency (that is, ability to minimize the number of records needed to reliably obtain these accurate median demand estimates) of ground motion scaling methods, including the effects of biased selection of ground motion records used in the analysis.

CURRENT PRACTICE AND CHALLENGES

Procedures for selecting and scaling ground motion records for a site-specific seismic hazard analysis are broadly described in current building codes. The ground motion selection and scaling procedures in IBC [25] and CBC [26] are based on ASCE 7-05 [27]. According to the ASCE provisions, the average 5%-damped linear-elastic acceleration response spectrum for a set of scaled records should not be less than the design spectrum over the period range from $0.2T_1$ to $1.5T_1$, where T_1 is the fundamental vibration period of the structure being designed. The design value of an engineering demand parameter (EDP) — member deformations, lateral displacements, floor accelerations, etc. — is taken as the average value of the EDP if seven or more records are used in the analysis, or its maximum value over all ground motions if the structure is analyzed for less than seven records (ASCE 7-05 requires a minimum of 3 records). These requirements are the same as those in ASCE 7-10 [28]. The required number of records prescribed by ASCE-7 is based on engineering judgment instead of a comprehensive evaluation [29].

Scaling methods that result in inaccurate estimates of the median EDPs with significant dispersion in the demands from the individual records in an ensemble can drastically alter the

For Peer Review

design outcome depending on the records selected, thus diminishing engineering confidence. To demonstrate the challenges for current practice, Figure 1 shows the measured peak roof drift demands, Δ_r (i.e., peak lateral displacement, D_r divided by the height to the roof) for one of the test structures described in this paper (Frame LE2) subjected to a suite of 25 ground motion records satisfying the ASCE 7-10 [28] scaling requirement. The ground motion intensity is plotted on the *x*-axis using the spectral acceleration of each ground motion at the fundamental period of the structure, $S_a(T_1)$ at a structural damping value of 5%. It can be seen that the drift demands from the ground motion records range from a minimum of slightly less than 0.1% to a maximum of about 1.2%. It is clear that if only the peak demand from 3 records were used in design, as allowed by ASCE 7-10, then the design outcome (i.e., over-design, under-design, satisfactory) can be drastically altered depending on the records selected. Although the use of a large number of records may improve the median EDP estimates, this approach may not be practical. Furthermore, the use of a large number of records does not answer the question on how these records should be scaled for a given design scenario. Thus, there is a need to develop the knowledge to achieve reliable demand estimates from RHA used in seismic design and assessment. This paper focuses on this issue.

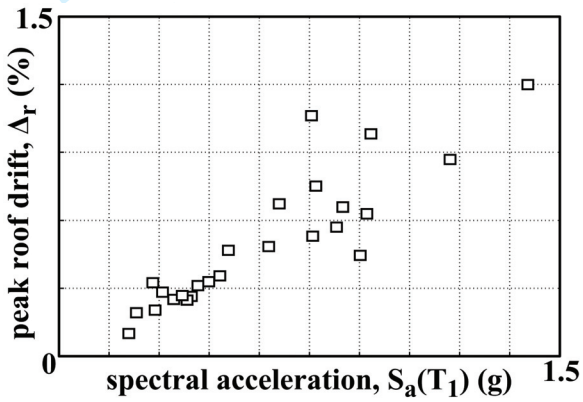

Figure 1. Peak roof drift, Δ_r demands for Frame LE2.

BACKGROUND

Previous research on ground motion scaling has primarily focused on "intensity-based" methods over "spectral matching." Spectral matching methods modify the frequency content or phasing of the record to match its response spectrum to a target spectrum, whereas intensity-based methods preserve the original non-stationary content of the ground motion record and only modify its amplitude using one or more intensity measures (IMs) to determine the appropriate scaling factors. The earliest approach to the problem is the scaling of ground motions to match a target peak ground acceleration (*PGA*), which has been shown to produce inaccurate median EDP estimates with large dispersion [2,3,4,12]. Other scalar IMs such as the effective peak acceleration, Arias intensity, and effective peak velocity have also been found inaccurate and inefficient [15]. On the other hand, the maximum incremental velocity (*MIV*, defined as the maximum area under the acceleration time-history of a ground motion between two consecutive zero acceleration crossings), which captures the impulsive characteristics of a ground motion record, can be a good indicator of the seismic demands [15,30-32].

None of the above IMs consider any property of the structure being designed in determining the ground motion scaling factors. Including a vibration property of the structure can lead to improved methods. For example, scaling records to a target linear-elastic spectral acceleration, $S_a(T_1)$ at the fundamental period of the structure, T_1, can provide improved EDP estimates for structures whose response is dominated by their first mode of vibration [13]. However, it has been shown that this scaling method becomes less accurate and less efficient for taller structures with significant higher mode response or for structures responding far into the nonlinear range [15,16]. To consider higher mode response, a scalar IM that combines the spectral accelerations $S_a(T_1)$ and $S_a(T_2)$ at the first two periods, as well as a vector IM based on $S_a(T_1)$ and the $S_a(T_1)/S_a(T_2)$ ratio have been studied [6]. While this vector IM improves accuracy, it remains inefficient for near-fault records with a dominant velocity pulse.

GROUND MOTION RECORDS AND SCALING METHODS

Due to a lack of specific guidelines, practitioners often select ground motion records based solely on distance, site conditions, and magnitude of the characteristic event expected to dominate the seismic hazard. However, many other factors, such as rupture directivity and/or basin effects contribute to the intensity and frequency content of a ground motion at a site. For example, as described in Kalkan and Kunnath [33,34], "forward directivity" and "fling-step" motions with long-period, large-amplitude pulses may impose large displacement demands that need to be dissipated in a single or relatively few response cycles of the structure.

For the selection of the ground motions in this study, a set of criteria and identification algorithms [35] were adopted to distinguish earthquake records based on their characteristic attributes associated with source, directivity, site, and/or basin effects (e.g., cyclic versus impulsive records; records with high, mid, or low frequency content; short or long duration records). Basin, duration, and pulse attributes of the records were investigated by frequency domain analyses; whereas, directivity and fling attributes were identified from the orientation of accelerometers relative to the fault strike. These attributes were then used to categorize a large library of records [36] to facilitate the selection of the most suitable ground motions for different site-specific hazard conditions. Based on this refinement and pre-selection process, a suite of 39 near-fault strong ground motions, recorded within 20 km of the causative fault in shallow-crustal tectonic environments, were compiled as shown in Table 1. Note that while all 39 records were used in the analytical investigation, only the 25 records in the gray shaded rows of Table 1 were used in the shake table experiments described in this paper.

Based on the records in Table 1, the following 6 suites of ground motions were utilized in this research:

- GM[Uns] – Unscaled ground motions from Table 1;
- GM[ASCE7] – Ground motions in Table 1 scaled based on ASCE 7-10 [28];
- GM[*MIV*] – Ground motions in Table 1 scaled to the median *MIV* of the suite;
- GM[$S_a(T_1)$] – Ground motions in Table 1 scaled to the median linear-elastic single-degree-of-freedom spectral acceleration at the fundamental period of the structure, T_1;
- GM[$S_a(1.3T_1)$] – Ground motions in Table 1 scaled to the median linear-elastic spectral acceleration at $1.3T_1$;
- GM[$S_a(0.7T_1)$] – Ground motions in Table 1 scaled to the median linear-elastic spectral acceleration at $0.7T_1$.

For Peer Review

Table 1. Selected near-fault ground motion records.

Record ID	Earthquake Name	Station Name	Year	Magnitude M_w	Fault Dist. (km)	V_{S30} (m/s)	*PGA* (g)	*MIV* (m/s)
1058-E	Duzce, Turkey	Lamont 1058	1999	7.1	0.2	425	0.111	0.256
1059-N	Duzce, Turkey	Lamont 1059	1999	7.1	4.2	425	0.147	0.103
1061-E	Duzce, Turkey	Lamont 1061	1999	7.1	11.5	481	0.134	0.144
1062-E	Duzce, Turkey	Lamont 1062	1999	7.1	9.2	338	0.257	0.256
375-N	Duzce, Turkey	Lamont 375	1999	7.1	3.9	425	0.970	0.612
531-N	Duzce, Turkey	Lamont 531	1999	7.1	8	660	0.159	0.160
BOL090	Duzce, Turkey	Bolu	1999	7.1	12	326	0.822	1.237
DZC270	Duzce, Turkey	Duzce	1999	7.1	6.7	276	0.535	1.108
A-CTR270	Irpinia, Italy	Calitri	1980	6.9	17.6	600	0.176	0.348
AMA090	Kobe, Japan	Amagasaki	1995	6.9	11.3	256	0.363	0.825
FKS090	Kobe, Japan	Fukushima	1995	6.9	17.9	256	0.216	0.543
KJM000	Kobe, Japan	KJMA	1995	6.9	1	312	0.821	1.586
NIS090	Kobe, Japan	Nishi-Akashi	1995	6.9	7.1	609	0.503	0.588
PRI000	Kobe, Japan	Port Island (0 m)	1995	6.9	3.3	198	0.315	1.494
SHI000	Kobe, Japan	Shin-Osaka	1995	6.9	19.1	256	0.243	0.501
TAK090	Kobe, Japan	Takatori	1995	6.9	1.5	256	0.616	1.862
TAZ090	Kobe, Japan	Takarazuka	1995	6.9	0.3	312	0.694	1.050
BRN090	Loma Prieta, CA	BRAN	1989	6.9	10.7	376	0.501	0.710
CAP000	Loma Prieta, CA	Capitola	1989	6.9	15.2	289	0.529	0.625
CLS000	Loma Prieta, CA	Corralitos	1989	6.9	3.9	463	0.644	0.829
G02000	Loma Prieta, CA	Gilroy Array #2	1989	6.9	11.1	271	0.367	0.507
G03000	Loma Prieta, CA	Gilroy Array #3	1989	6.9	12.8	350	0.555	0.537
G04000	Loma Prieta, CA	Gilroy Array #4	1989	6.9	14.3	222	0.417	0.547
G06090	Loma Prieta, CA	Gilroy Array #6	1989	6.9	18.3	664	0.170	0.208
GIL067	Loma Prieta, CA	Gilroy-Gavilan Coll.	1989	6.9	10	730	0.357	0.331
GOF160	Loma Prieta, CA	Gilroy-Historic Bldg.	1989	6.9	11	339	0.284	0.777
LGP090	Loma Prieta, CA	LGPC	1989	6.9	5	1070	0.605	0.615
LOB000	Loma Prieta, CA	UCSC Lick Observatory	1989	6.9	18.4	714	0.450	0.290
SJTE225	Loma Prieta, CA	San Jose-Santa Teresa Hills	1989	6.9	14.7	672	0.275	0.239
STG000	Loma Prieta, CA	Saratoga-Aloha Ave	1989	6.9	8.5	371	0.512	0.588
UC2090	Loma Prieta, CA	UCSC	1989	6.9	18.5	714	0.396	0.200
WAH090	Loma Prieta, CA	WAHO	1989	6.9	17.5	376	0.638	0.466
WVC270	Loma Prieta, CA	Saratoga-W Valley Coll.	1989	6.9	9.3	371	0.332	0.673
CPM000	Cape Mendocino, CA	Cape Mendocino	1992	7.0	7	514	1.497	1.196
FOR000	Cape Mendocino, CA	Fortuna-Fortuna Blvd	1992	7.0	19.9	457	0.116	0.372
PET090	Cape Mendocino, CA	Petrolia	1992	7.0	8.2	713	0.662	1.232
RIO360	Cape Mendocino, CA	Rio Dell Overpass-FF	1992	7.0	14.3	312	0.549	0.737
HEC090	Hector Mine, CA	Hector	1999	7.1	12	685	0.337	0.480
I-ELC180	Imperial Valley-02	El Centro Array #9	1940	6.9	6.1	213	0.313	0.462

Figure 2 shows the linear-elastic acceleration response spectra of the ground motion records in Suites GM[Uns], GM[*MIV*] as well as the records in Suites GM[ASCE7], GM[$S_a(T_1)$], GM[$S_a(1.3T_1)$], and GM[$S_a(0.7T_1)$] based on the fundamental period, T_1 of Frame LE2. The spectra are plotted using the measured viscous damping, ξ for Frame LE2 under each suite as described later. Note that with the exception of the *MIV*-scaled records, the other scaling methods investigated in this paper depend on T_1. Suites GM[$S_a(1.3T_1)$] and GM[$S_a(0.7T_1)$]

investigate the effects of uncertainties in structural period estimation (i.e., inaccuracies in period estimation that could be expected in typical design practice) by introducing a 30% error in T_1.

In applying the ASCE-7 scaling method, the ground motions were scaled such that the average 5%-damped linear-elastic acceleration response spectrum for the suite was not less than the median response spectrum of the unscaled records over the period range from $0.2T_1$ to $1.5T_1$. The median spectrum rather than a code-based design spectrum was used so as not to introduce any bias to the study. A different scaling factor was determined for each record in the GM[ASCE7] suite to minimize the SRSS error between the spectrum of the scaled record and the target median spectrum within the period range from $0.2T_1$ to $1.5T_1$. Note that the ASCE-7 method does not result in a unique scaling factor for each record; various combinations of scaling factors can be found to satisfy the requirement that the mean spectrum of the scaled records remains above the target spectrum over the specified period range. An algorithm, given in Appendix A of Kalkan and Chopra (2010), was used in determining the scaling factors for the GM[ASCE7] suite in this paper.

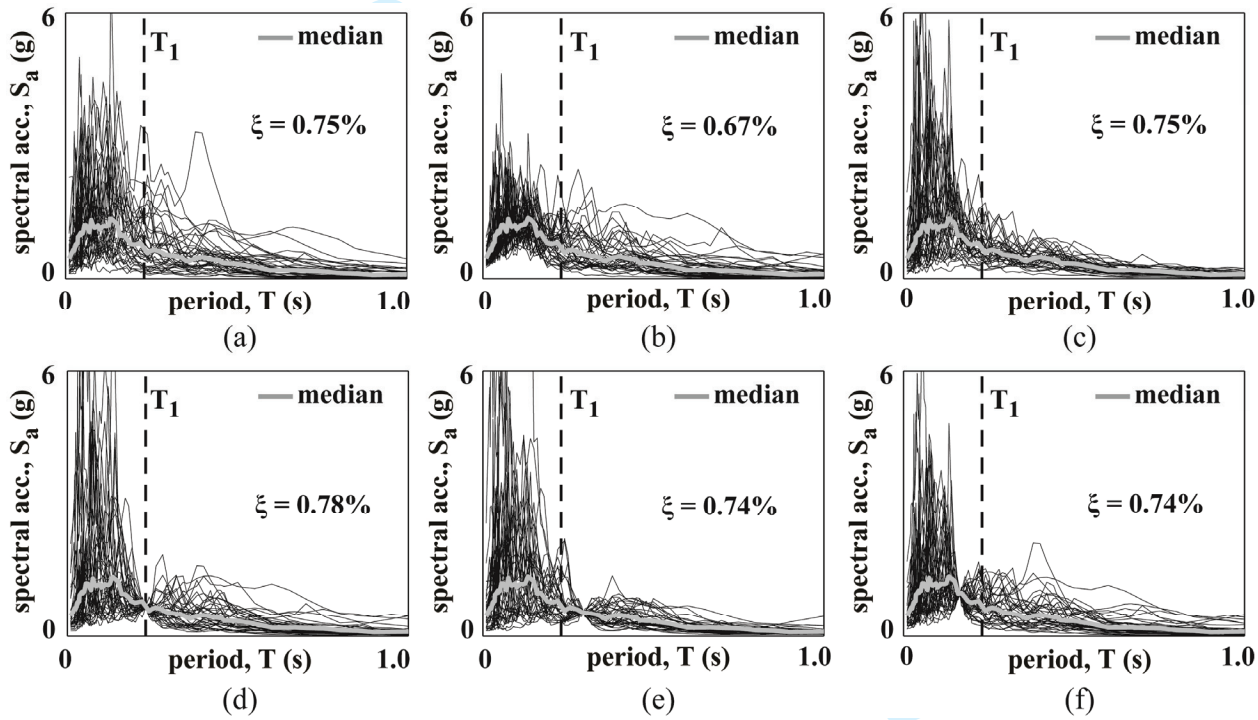

Figure 2. Linear-elastic acceleration response spectra, S_a: (a) GM[Uns]; (b) GM[ASCE7]; (c) GM[*MIV*]; (d) GM[$S_a(T_1)$]; (e) GM[$S_a(1.3T_1)$]; (f) GM[$S_a(0.7T_1)$].

TEST STRUCTURES

As shown in Figure 3(a), the frame structure configuration selected for the experimental investigation was a six-story single-bay system with center-to-center span length of 762 mm and story height of 432 mm. These dimensions correspond to a building length-scale of, approximately, S_L=1/10. The structure was subjected to the six ground motion suites described previously with a time-scale of S_T=1/3. The tests were conducted on a medium-size uniaxial shake table that consists of a hydraulic actuator/servo-valve assembly and a hydraulic power supply that drive a 1.2 m by 1.2 m slip table. Four different structure periods were investigated

by varying the amount of superimposed mass on the test frame as follows (using 21 kg steel mass plates attached to the midspan of each beam):

- Frame LE1 – one superimposed mass plate at each floor and roof level
- Frame LE2 – two mass plates at each floor and one plate at the roof
- Frame LE3 – three mass plates at each floor and one plate at the roof
- Frame LE4 – four mass plates at each floor and one plate at the roof

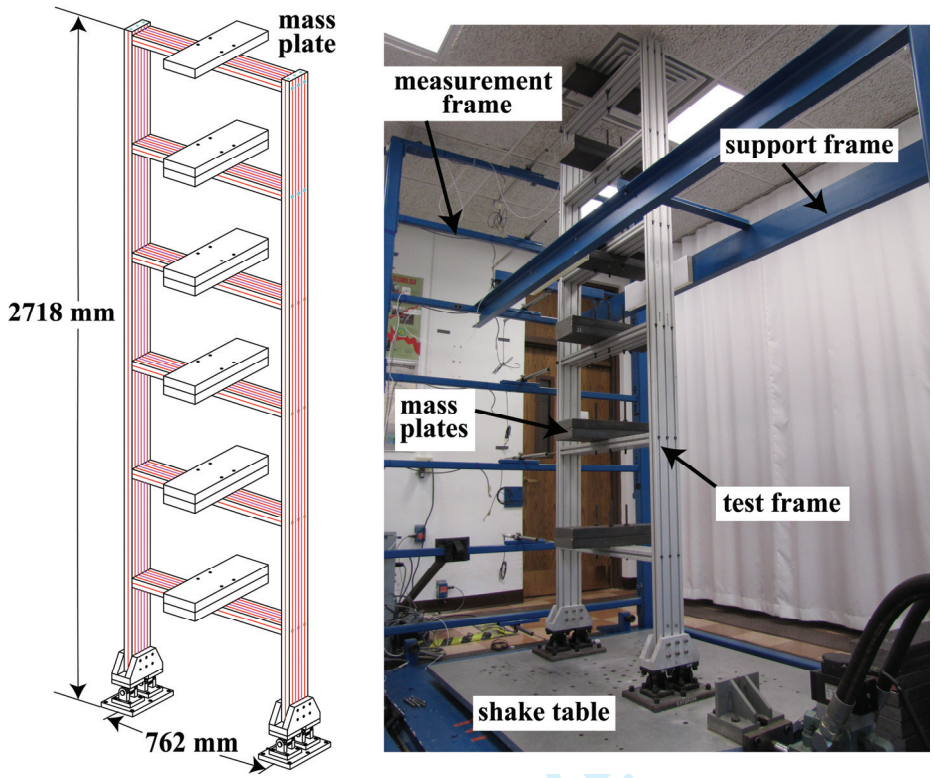

(a) (b)

Figure 3. Six-story test frame: (a) schematic; (b) test setup.

Figure 3(b) depicts Frame LE2 placed on the shake table, together with the measurement and out-of-plane bracing frames mounted onto the laboratory floor. The test frame was fabricated from extruded aluminum 6105-T5 alloy with a yield strength of 241 MN/m^2. The beam and column member cross-sections were determined to result in stiffness appropriate with the scale model and adequate strength to prevent yielding. The extruded aluminum cross-section in Figure 4(a), oriented in the weak direction (with moment of inertia, I=295524 mm^4 and area, A=1935 mm^2) was used for all beam and column members. To achieve a modular structure, each beam-column connection was constructed using three high-strength bolts passing through the column and screwing into holes tapped into the beam cross-section at each end. The column bases were constructed with pinned connections. Figure 4(b) depicts a close-up view of the pinned base connection, which consists of a steel plate bolted to the shake table top, two steel clevises bolted to the plate, and two steel eye brackets inserted into the clevises and bolted to an aluminum fixture at the column base. A tight tolerance greased steel pin was used through the eye bracket-to-clevis connection to reduce friction while eliminating backlash effects.

Two accelerometers were used to monitor the accelerations of the beam midspan at the roof and 4th floor level of the structure, and one additional accelerometer was placed directly on

the shake table. In addition to the table displacements, the displacements of the test structure were measured using seven free unguided LVDTs (six at the floor and roof levels and one at the base) anchored between the structure and a fixed measurement frame. A mounted LVDT can be seen in Figure 4(c). The clamps used to attach the LVDTs to the measurement frame were engineered to mitigate vibrations. The data was collected at a high sampling rate, resulting in close-to-simultaneous excitation and response measurements.

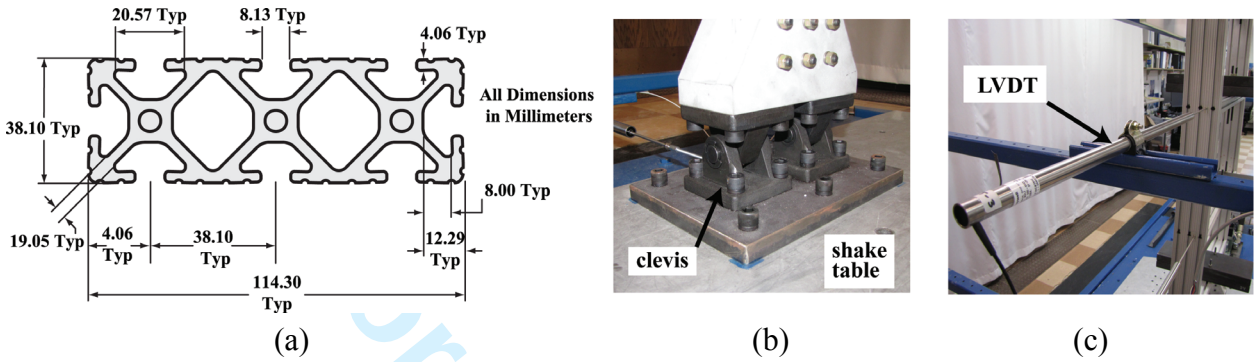

(a) (b) (c)

Figure 4. Test details: (a) extrusion profile for beam and column members (courtesy 80/20® Inc.); (b) pinned connection at column base; (c) LVDT mounted to measurement frame.

BEHAVIOR OF TEST STRUCTURE UNDER STATIC LOADING

To determine the lateral load versus displacement behavior of the test structure under static loading, monotonic and reversed-cyclic pushover experiments were conducted by holding the 4th floor of the frame stationary while slowly displacing the base using the shake table. At the 4th floor level, a steel rod with pin-ended connections [Figure 5(a)] was placed between the test structure and a relatively stiff steel loading frame. As the base of the structure was displaced, the resulting 4th floor force in the pin-ended rod was measured using an intermediary load cell. Two string pot transducers were used to measure the absolute lateral displacements at the base and 4th floor level of the structure (note that the 4th floor displacements were very small but not zero due to the deformations of the loading frame).

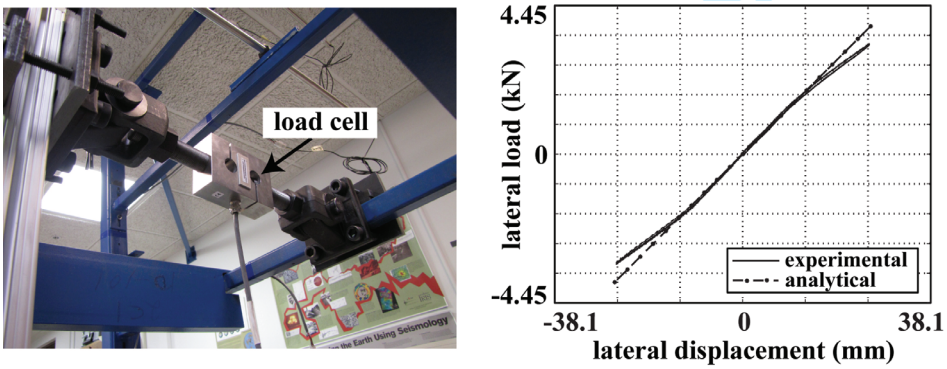

(a) (b)

Figure 5. Static tests: (a) pin-ended rod and load cell assembly; (b) lateral load versus displacement behavior.

The 4th floor lateral force versus relative (with respect to base) displacement behavior of the frame during two cycles of loading is shown using the thin black lines in Figure 5(b). The structure exhibited consistent and repeatable behavior in both the positive and negative loading directions, with a small amount of nonlinearity beginning at approximately 13 mm relative displacement. The nonlinear behavior occurred as the beam ends lost full contact with the columns due to the stretching of the beam-column connection bolts. The flexibility of the connection bolts also reduced the initial lateral stiffness of the frame (i.e., the beam-to-column connections were not perfectly rigid).

DYNAMIC CHARACTERISTICS OF TEST FRAMES

The dynamic characteristics of Frames LE1, LE2, LE3, and LE4 were measured by subjecting the structures to a series of sine-sweep tests. The results from three series of sine-sweep tests on Frame LE2 with base excitation amplitudes ranging from 0.13 mm to 0.38 mm can be seen in Figure 6(a), where the *y*-axis shows the ratio of the relative roof displacement amplitude to the base excitation amplitude and the *x*-axis shows the frequency of the sine wave exciting the structure. While some amplitude-dependency was observed in the results, the fundamental frequencies were found as f_1= 5.32, 4.35, 3.82, and 3.42 Hz for Frames LE1, LE2, LE3, and LE4, respectively (corresponding to periods of T_1=0.19, 0.23, 0.26, and 0.29 s, respectively). With the selected time-scale of S_T=1/3, the test specimens correspond to full-scale structures with fundamental periods of T_1=0.56, 0.69, 0.79, and 0.88 s, respectively. The measured mode shapes for Frame LE2 in the first two modes of vibration can be seen in Figure 6(b).

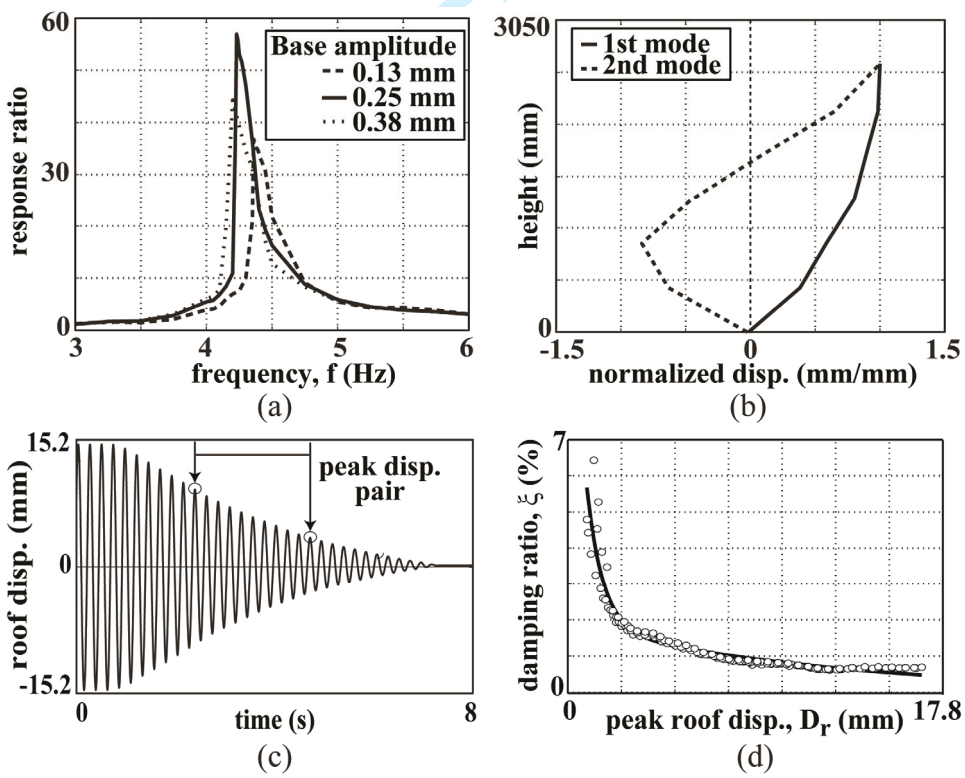

Figure 6. Dynamic characteristics of Frame LE2: (a) resonance peaks; (b) first and second mode shapes; (c) decay of roof displacement response; (d) displacement-dependent damping.

The damping ratio for each structure was determined using the logarithmic decrement method [37] on the decay of the measured displacement response at the roof. The logarithmic decrement method was applied to a series of peak roof displacement pairs with decreasing amplitudes, each pair 10 cycles apart as shown on the typical roof displacement time-history for Frame LE2 in Figure 6(c). As can be seen in Figure 6(d), a correlation was evident between the amplitude of the peak roof displacement and the amount of damping exhibited by the structure. For use in the dynamic response history analyses described later in the paper, a displacement-dependent damping regression line [e.g., solid line in Figure 6(d)] was fit to the data for each structure (slight differences were observed in the damping regression lines for the four test frames).

ANALYTICAL MODELING

As shown in Figure 7, analytical models of the test structures were developed using the OpenSEES [38] and DRAIN-2DX [39] programs. The extruded aluminum cross-section in Figure 4(a) was modeled using fiber cross-sections for the beam and column members. The column bases were modeled as pinned and the flexibility of the beam-column connections (due to the flexibility of the connection bolts) was modeled by placing linear-elastic zero-length rotational springs at the beam ends. The stiffness of the rotational springs was determined by calibrating the model results [dashed-dotted line in Figure 5(b)] with the linear-elastic range of the measured lateral load versus displacement behavior of the structure.

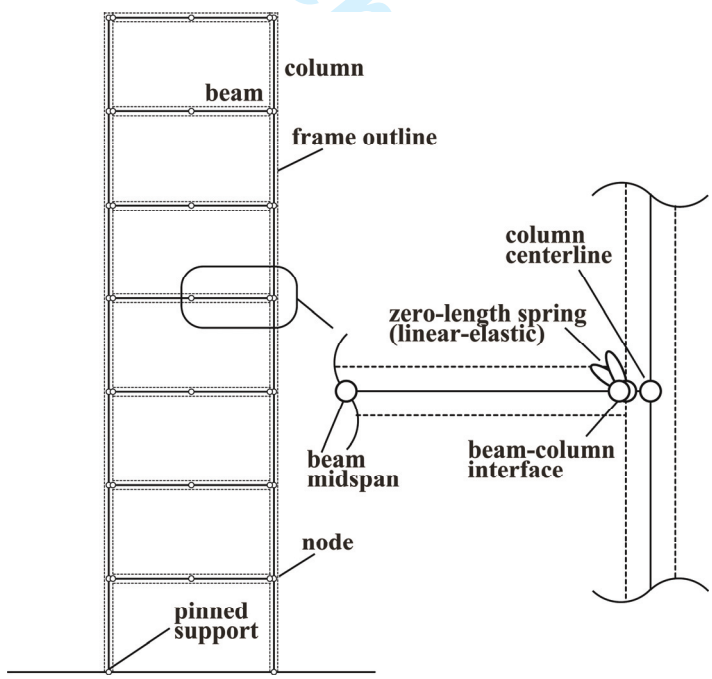

(a) (b)

Figure 7. Analytical modeling: (a) overall model; (b) beam-column joint region.

Modal analyses of the analytical models revealed excellent comparisons with the measured first mode shapes and frequencies for all four test structures. In addition, response

history analysis results for the structures were compared with measured dynamic response histories. For example, analytical and measured roof displacement response comparisons for the OpenSEES model of Frame LE2 under two unscaled ground motion records from Table 1 can be seen in Figure 8. Once the accuracy of the analytical results was deemed sufficient, the OpenSEES model was integrated with a Matlab® script to subject the structures to the six suites of ground motion records and to guide the shake table tests described in the next section. A slightly different damping ratio was used for each structure analyzed under each ground motion suite, as determined from the displacement-dependent damping regression line [e.g., solid line in Figure 6(d)] at the median peak roof displacement of the structure under that suite.

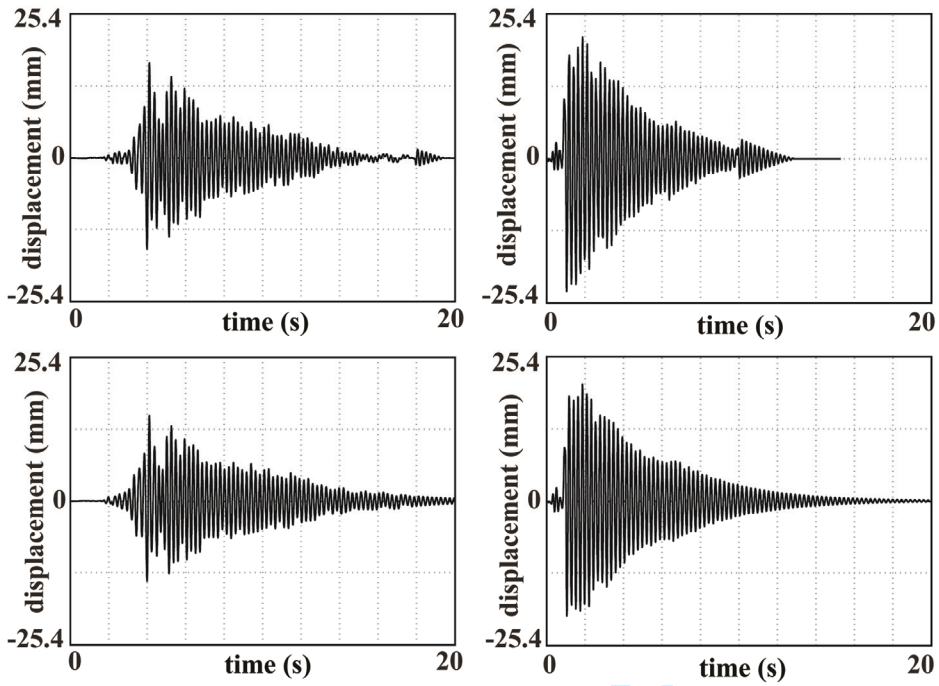

(a) (b)

Figure 8. Measured (top) and analytical (bottom) roof displacement responses of Frame LE2: (a) STG000; (b) CPM000.

EFFECT OF GROUND MOTION SCALING

With the characteristics of Frames LE1, LE2, LE3, and LE4 fully understood and the expected displacement demands from the ground motions in each suite estimated by the calibrated analytical models, the test specimens were subjected to the series of shake table experiments. For each structure, the pre-test analyses indicated several ground motion records likely to subject the frame through significant nonlinear displacements. These ground motion records were excluded from the experimental investigation, resulting in 25 records that were common to the testing of the four structures (gray shaded rows in Table 1). The peak roof drift (Δ_r) demands from the six series of experiments for each structure are plotted in Figure 9 (note that the absolute values are used for all demands). It can be seen that the peak displacement demands from the GM[Uns] suite (■ markers) are not as strongly correlated to *MIV* as compared to the correlation with S_a.

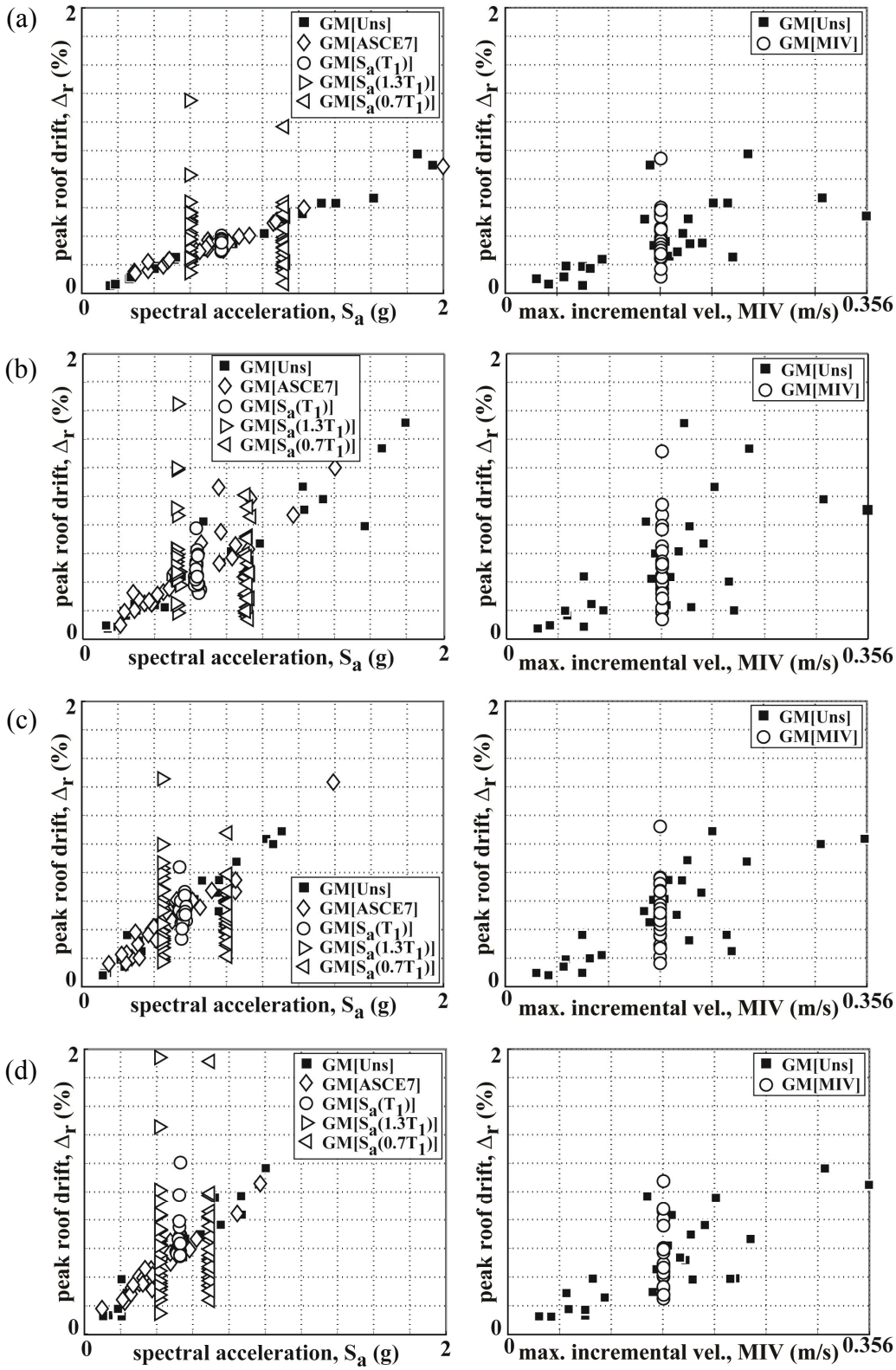

Figure 9. Peak roof drift, Δ_r demands plotted against S_a and *MIV*: (a) Frame LE1; (b) Frame LE2; (c) Frame LE3; (d) Frame LE4.

The median peak roof drift demand, $\hat{\Delta}_r$ as well as the coefficient of variation, COV of the peak roof drift demands for Frames LE1, LE2, LE3, and LE4 under each ground motion suite are listed in Table 2 (note that in addition to the test frames, Table 2 includes results from an analytical study described in the next section). The COV measure, defined as the ratio between the sample standard deviation and the sample mean, is used to assess the effectiveness of the scaling methods in reducing the dispersion in the peak demands. As can be expected for a linear-elastic structure, the $S_a(T_1)$ scaling method produced the smallest dispersion in the peak roof drift demands. However, the dispersion more than doubled when a 30% error was introduced in period estimation, resulting in values greater than the dispersion from the *MIV*-scaled suite. These results are important in showing that, for structures with limited nonlinearity, inaccuracies in the estimation of a structure's period can lead to a much larger dispersion in the seismic demand estimates when compared with the dispersion achieved with the records scaled based on the "exact" period. Ground motion scaling methods that are not dependent on the properties of the structure, such as scaling based on the *MIV*, not only result in a simpler procedure (since the same scaled ground motion set could be used for different buildings with similar site and seismic hazard characteristics) but may also produce less uncertainty in the estimated seismic demands. Out of the methods investigated in this paper, the ASCE-7 scaling method was the least consistent and least effective in reducing the dispersion in the peak roof drift demands of the four test structures, exhibiting a wide COV range from 0.47 to 0.79. For Frame LE4, the dispersion produced from the ASCE-7 method even surpassed that of the unscaled suite.

Table 2. Summary results for peak roof drift demands.

T_1 (s)	GM[Uns]		GM[ASCE7]		GM[*MIV*]		GM[$S_a(T_1)$]		GM[$S_a(1.3T_1)$]		GM[$S_a(0.7T_1)$]	
	$\hat{\Delta}_r$ (%)	COV(Δ_r)	$\hat{\Delta}_r$ (%)	COV(Δ_r)	$\hat{\Delta}_r$ (%)	COV(Δ_r)	$\hat{\Delta}_r$ (%)	COV(Δ_r)	$\hat{\Delta}_r$ (%)	COV(Δ_r)	$\hat{\Delta}_r$ (%)	COV(Δ_r)
0.15	0.335	0.656	0.294	0.409	0.371	0.409	0.286	0.083	0.305	0.427	0.291	0.501
0.19 (LE1)	0.347	0.637	0.309	0.466	0.345	0.449	0.352	0.087	0.408	0.573	0.317	0.631
0.23 (LE2)	0.435	0.748	0.445	0.588	0.447	0.526	0.439	0.225	0.482	0.558	0.435	0.533
0.26 (LE3)	0.503	0.622	0.420	0.563	0.515	0.393	0.537	0.179	0.440	0.565	0.497	0.350
0.29 (LE4)	0.454	0.593	0.414	0.786	0.492	0.385	0.630	0.222	0.615	0.621	0.508	0.580
0.43	0.864	0.614	0.899	0.508	0.996	0.440	0.976	0.089	1.021	0.551	1.229	0.370
0.53	0.955	0.558	1.032	0.511	1.211	0.415	0.988	0.146	1.179	0.452	1.083	0.402
0.66	0.729	0.705	0.780	0.614	0.858	0.544	0.932	0.125	1.039	0.280	0.798	0.559
0.81	0.616	0.688	0.827	0.402	0.795	0.447	0.960	0.158	0.893	0.469	0.824	0.329
1.00	1.021	0.655	1.105	0.592	0.967	0.533	1.064	0.157	1.158	0.451	1.157	0.593

Note: The results shown for Frames LE1, LE2, LE3, and LE4 are test data. The corresponding analytical results were found to be very similar.

ANALYTICAL EXTENSION OF RESULTS

This section uses the validated analytical models of the test frames to extend the shake table results over a wider range of parameters. First, the superimposed floor and roof masses of the 6-story OpenSEES model were varied to result in a series of 10 analytical structures with fundamental periods exponentially spaced between T_1=0.15 s to 1.00 s (four of the selected periods matched the measured periods of Frames LE1 through LE4 for the validation of the results). This analytical period range, which corresponds to full-scale structural periods of 0.45 s to 3.00 s, is representative of a much wider range of buildings, including tall structures. The structures were

analyzed under the 6 suites of ground motions using the 25 records that were common to the testing of Frames LE1-LE4 (gray shaded rows in Table 1). As listed in Table 2 and shown in Figure 10, the dispersion in the resulting peak roof drift demands can be visualized as COV spectra from each ground motion suite. As may be expected for a linear-elastic structure, the dispersion from the $S_a(T_1)$ scaling method (* markers in Figure 10) consistently outperformed the other scaling methods throughout the entire range of periods. The unscaled suite (thick solid line with □ markers) produced the largest dispersion in the peak roof drift of 9 of the 10 structures, with the GM[ASCE7] (thick dotted line with ◊ markers), GM[$S_a(1.3T_1)$], GM[$S_a(0.7T_1)$], and GM[*MIV*] (thick dashed line with Δ markers) suites producing, on average, less dispersion in order of improved performance. These results confirm the potential vulnerabilities of structure-dependent ground motion scaling methods over a wider range of structure periods.

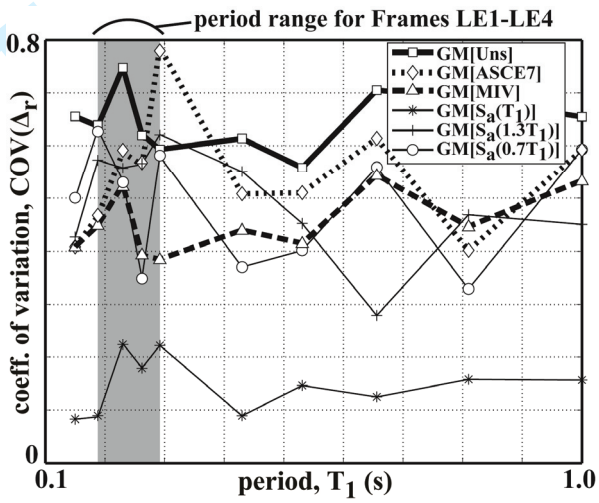

Figure 10. Dispersion in peak roof drift demand, $\mathrm{COV}(\Delta_r)$ over a range of fundamental periods (Note: results shown for Frames LE1, LE2, LE3, and LE4 are test data).

As a second analytical study, the OpenSEES model was extended to include 4-story and 14-story structures in addition to the 6-story structure that was tested. The superimposed mass was held constant at 2 mass plates per floor and one plate on the roof, resulting in scaled fundamental periods of T_1=0.16, 0.23, and 0.52 s for the 4-, 6-, and 14-story structures, respectively (corresponding to full-scale periods of 0.47, 0.69 and 1.55 s, respectively). The focus of this study was the "accuracy" of the ground motion scaling methods (that is, ability to provide accurate estimates of the median peak demands as if a much larger set of records were used). Thus, for each structure and scaling method, 9 subset ground motion bins were selected, each bin containing 7 records from the complete set of 39 records. Bins 1-3 were chosen randomly from the full set but an intentional bias was introduced into the remaining 6 subsets. For these subsets, Bins 4-6 were selected with a weak ground motion bias and Bins 7-9 were selected with a strong ground motion bias. To introduce this bias, the 39 ground motion records were sorted by ascending peak roof drift demand for each structure and the ground motions were either selected from below the median roof drift to introduce a weak bias or from above the median roof drift to introduce a strong bias.

The accuracy of the scaling methods was evaluated using the inter-story drift ratio, $r(\hat{\delta})$, defined as the ratio between the median inter-story drift demand, $\hat{\delta}_s$ from each subset ground motion bin divided by the benchmark demand determined as the median inter-story drift demand, $\hat{\delta}_b$ from the full unscaled suite of 39 ground motions. The dispersion in the peak inter-story drift

demands, $\mathrm{COV}(\delta)$ was also calculated for each ground motion bin. The variation in $r(\hat{\delta})$ and $\mathrm{COV}(\delta)$ over the height of the 6-story frame (i.e., analytical model for Frame LE2) for the 9 ground motion bins can be seen in Figures 11 and 12, respectively.

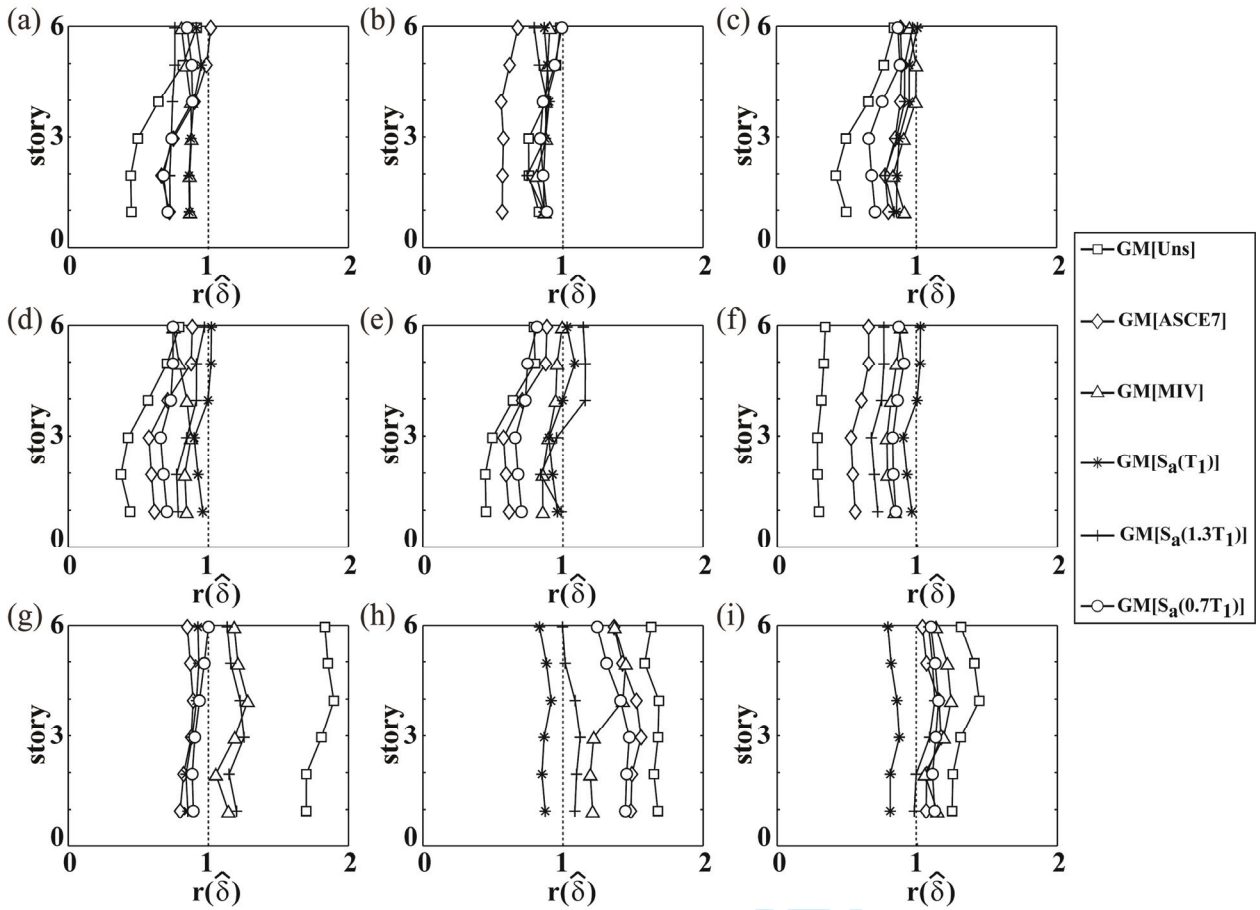

Figure 11. Inter-story drift ratio, $r(\hat{\delta})$ for the 6-story frame: (a-i) Bins 1-9.

In Figure 11, a value of 1.0 for $r(\hat{\delta})$ indicates perfect accuracy where the median inter-story drift demand from the subset bin, $\hat{\delta}_s$ matches that of the unscaled full suite of ground motion records, $\hat{\delta}_b$. To quantify an overall measure of accuracy, the average absolute error in the median inter-story drift demand, $|\bar{E}(\hat{\delta})|$ was calculated for each bin by dividing the sum of the absolute error, $|E(\hat{\delta})| = |r(\hat{\delta}) - 1|$ values by the number of stories over the height. Similarly, the average dispersion in the inter-story drift was calculated as $\overline{\mathrm{COV}}(\delta)$. Finally, to determine whether a scaling method was more likely to overestimate or underestimate the median demands, the maximum and minimum errors, $E_m(\hat{\delta}) = \max \text{and} \min[\, r(\hat{\delta}) - 1]$ in the median inter-story drift demands over the height of each structure were also calculated. Positive values of $E_m(\hat{\delta})$ indicate an overestimation of the median inter-story drift demand relative to the benchmark drift demand, potentially leading to an uneconomical design. Conversely, negative values of $E_m(\hat{\delta})$ represent an underestimation of the median inter-story drift demand, potentially leading to an unconservative design.

The $|\bar{E}(\hat{\delta})|$, $\overline{\mathrm{COV}}(\delta)$, and $E_m(\hat{\delta})$ results for the 4-, 6-, and 14-story structures are plotted as bar graphs in Figures 13, 14, and 15. All three sets of results need to be taken into consideration to evaluate the effectiveness of a scaling method. For example, looking at Figure 14(b) for the 6-story structure, the $\overline{\mathrm{COV}}(\delta)$ value under Bin 7 from the unscaled ground motion suite is relatively small (indicating low dispersion in the inter-story drift demands). However, the $|\bar{E}(\hat{\delta})|$ and $E_m(\hat{\delta})$ values for the same bin are very large [Figures 13(b) and 15(b)], indicating poor accuracy in the results.

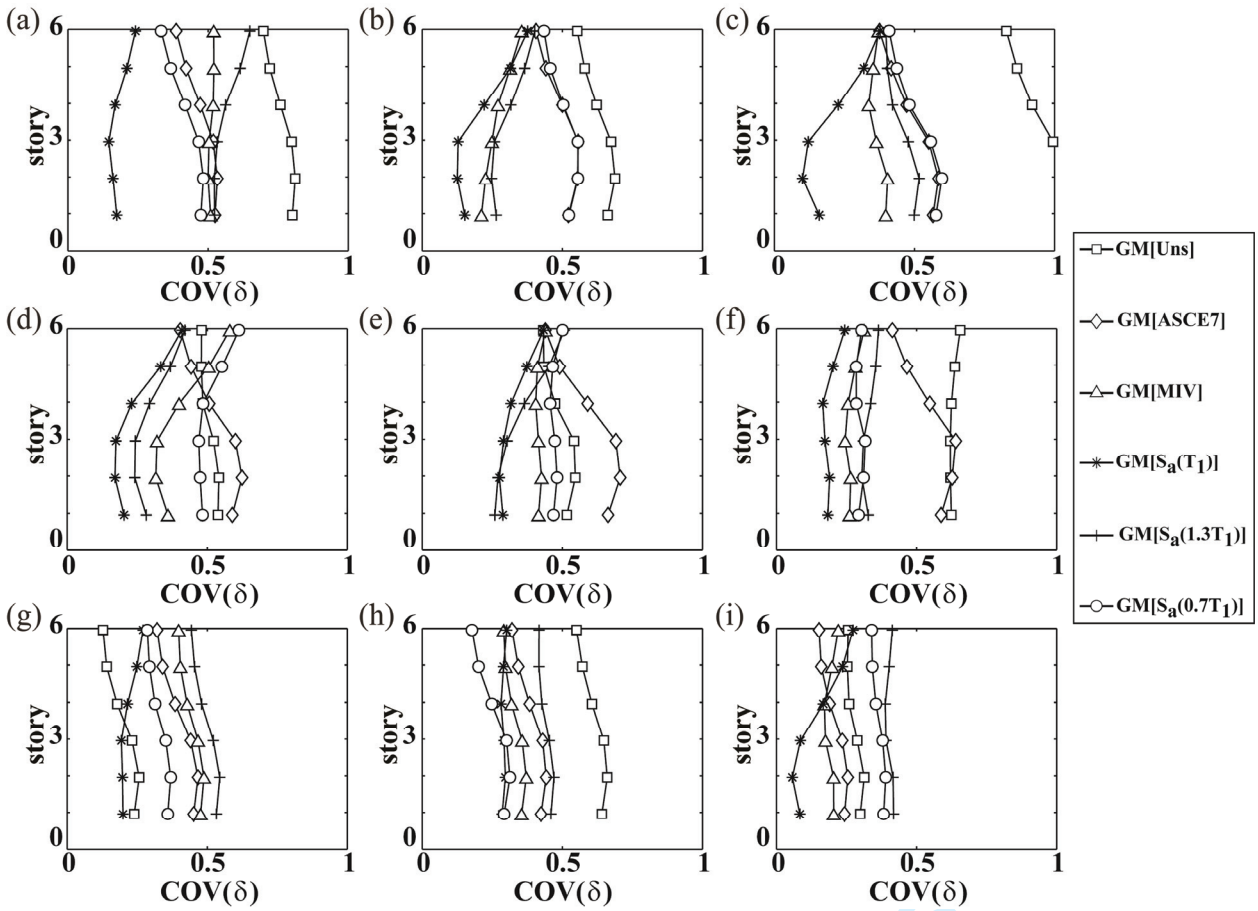

Figure 12. Dispersion in inter-story drift demands, $\mathrm{COV}(\delta)$ for the 6-story frame: (a-i) Bins 1-9.

While there is considerable variability in the results between the different bins, it can be seen in Figures 13, 14, and 15 that, on average, the $S_a(T_1)$ scaling method was more effective in minimizing bin dispersion, $\overline{\mathrm{COV}}(\delta)$, and error, $|\bar{E}(\hat{\delta})|$ and $E_m(\hat{\delta})$. However, inaccuracies in period estimation can erode the effectiveness of the $S_a(T_1)$ method as demonstrated by the relatively poor performance of the $S_a(1.3T_1)$ and $S_a(0.7T_1)$ methods. The ASCE-7 and *MIV* scaling methods performed similarly for the 4- and 14-story structures but the *MIV* method was, on average, more effective than the ASCE-7 method for the 6-story structure. Note that although the ASCE-7 method requires scaling based on a range of structural periods [rather than only the fundamental period as required for the $S_a(T_1)$ method], this period range is still based on an estimate of the fundamental period thus making the ASCE-7 method susceptible to similar shortcomings as the $S_a(T_1)$ method. It may therefore be more advantageous to use the *MIV*

method, which is structure-independent and can be applied to a ground motion suite without the need to estimate the fundamental period of the structure. Any changes in the building properties would not require the scaled ground motion records to be iterated.

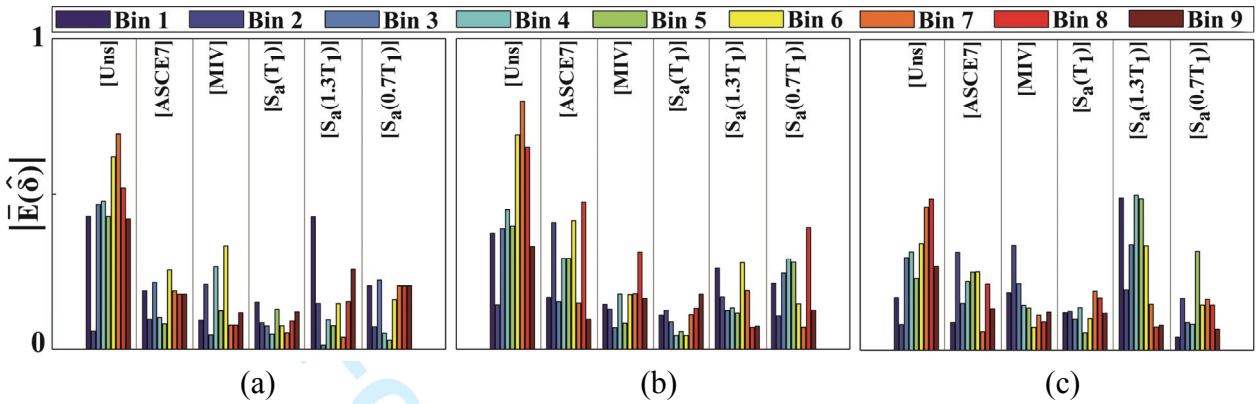

Figure 13. Average absolute error in median inter-story drift demands, $|\bar{E}(\hat{\delta})|$ for Bins 1-9: (a) 4-story frame; (b) 6-story frame; (c) 14-story frame.

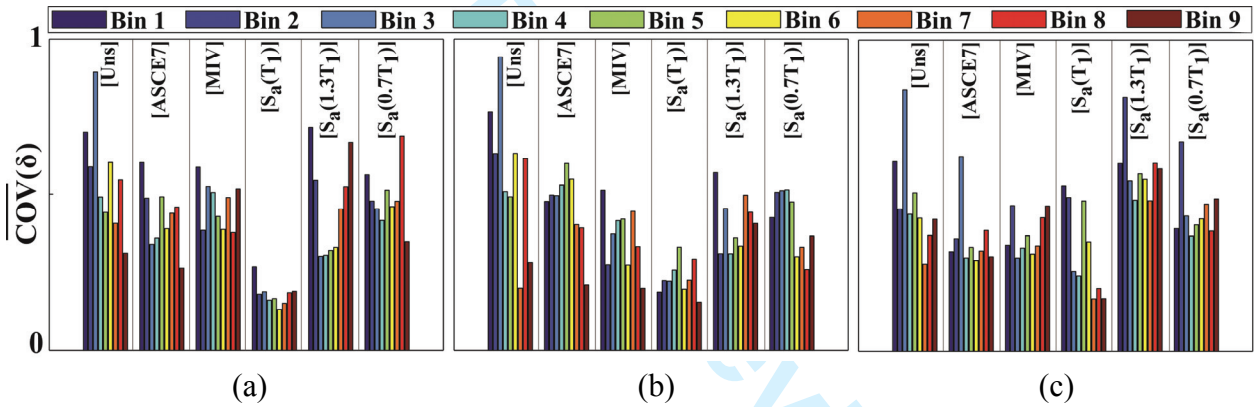

Figure 14. Average dispersion in inter-story drift demands, $\overline{\mathrm{COV}}(\delta)$ for Bins 1-9: (a) 4-story frame; (b) 6-story frame; (c) 14-story frame.

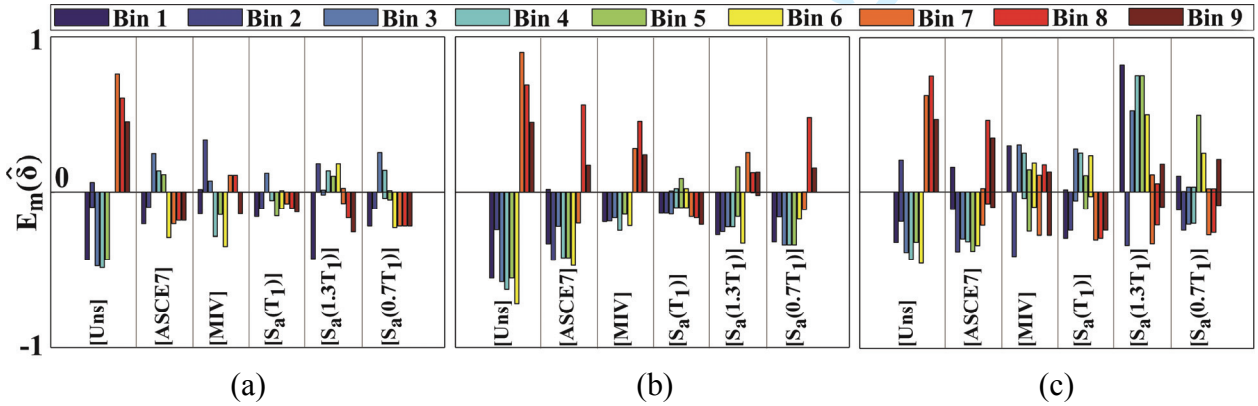

Figure 15. Maximum and minimum errors in median inter-story drift demands, $E_m(\hat{\delta})$ for Bins 1-9: (a) 4-story frame; (b) 6-story frame; (c) 14-story frame.

SUMMARY AND CONCLUSIONS

This paper describes an integrated experimental and analytical evaluation of selected ground motion scaling methods for use in the response history analysis of building frame structures exhibiting limited nonlinearity. The general experimental setup and the features of a 1/10-scale 6-story linear-elastic test frame specimen are presented, along with the identification results for the static and dynamic properties of the structure. To extend the applicability of the experimental results, an analytical model was calibrated to the test structure and two separate analytical parameter studies were conducted to investigate the scaling methods over a wider range of building properties. The effectiveness of the scaling methods was evaluated by determining the dispersion in the peak roof drift and inter-story drift demands of the structures, as well as the accuracy in the median demands when a smaller subset of ground motion records was used, including the effects of biased selection of these records. Although the $S_a(T_1)$ scaling method was most effective in minimizing dispersion and maximizing accuracy, it was found that inaccuracies in the estimation of the fundamental period, T_1 of the structure could erode this effectiveness as demonstrated by the relatively poor performance of the $S_a(1.3T_1)$ and $S_a(0.7T_1)$ methods. For structures with limited nonlinearity, these results stress the potential uncertainty from scaling methods that are based on the knowledge of the exact properties of the structure. The ASCE-7 and *MIV* scaling methods performed similarly for the 4- and 14-story structures but the *MIV* method was, on average, more effective than the ASCE-7 method for the 6-story structure. It may be more advantageous to use the *MIV* scaling method, which is structure-independent and can be applied to a ground motion suite without the need to estimate the fundamental period of the structure being designed.

For Peer Review

ACKNOWLEDGEMENTS

This research is funded by the National Science Foundation (NSF) under Grant No. CMMI 0928662. The support of Dr. M.P Singh, former NSF Program Director, and Dr. K.I. Mehta, current NSF Program Director, is gratefully acknowledged. The authors would like to acknowledge the project advisory panel, which includes Paulo Bazzurro, AIR Worldwide Corporation, Sigmund Freeman, Wiss, Janney, Elstner Associates, Inc., Vladimir Graizer, U.S. Nuclear Regulatory Commission, Farzad Naeim, John A. Martin and Associates, Inc., and Thomas Sabol, Englekirk & Sabol Consulting Structural Engineers, Inc. The authors also thank Bob St. Henry of NEFF Engineering for his help in the design of the test structure. The opinions, findings, and conclusions in the paper are those of the authors and do not necessarily reflect the views of the organizations or individuals above.

REFERENCES

1. Kennedy R, Short S, Merz K, Tokarz F, Idriss I, Powers M, Sadigh K. Engineering characterization of ground motion-task I: Effects of characteristics of free-field motion on structural response. NUREG/CR-3805, U.S. Regulatory Commission, Washington, D.C., 1984.
2. Nau J, Hall W. Scaling methods for earthquake response spectra. *J. of Structural Engineering*, 110, 1984, 91-109.

3. Miranda E. Evaluation of site-dependent inelastic seismic design spectra. *J. of Structural Engineering*, 119(5), 1993, 1319-1338.
4. Vidic T, Fajfar P, Fischinger M. Consistent inelastic design spectra: strength and displacement. *Earthquake Engineering & Structural Dynamics*, 23, 1994, 507-521.
5. Martinez-Rueda J. Scaling procedure for natural accelerograms based on a system of spectrum intensity scales. *Earthquake Spectra*, 14, 1998, 135-152.
6. Shome N, Cornell C. Probabilistic seismic demand analysis of nonlinear structures. Reliability of Marine Structures Program Report No. RMS-35, Department of Civil and Environmental Engineering, Stanford University, CA, 1999.
7. Baez J, Miranda E. Amplification factors to estimate inelastic displacement demands for the design of structures in the near field. *12th World Conference on Earthquake Engineering*, Paper No. 1561, Auckland, New Zealand, 2000.
8. Malhotra P. Strong-motion records for site-specific analysis. *Earthquake Spectra*, 19(3), 2003, 557-578.
9. Naeim F, Alimoradi A, Pezeshk S. Selection and scaling of ground motion time histories for structural design using genetic algorithms. *Earthquake Spectra*, 20(2), 2004, 413-426.
10. Luco N, Cornell A. Structure-specific scalar intensity measures for near-source and ordinary earthquake ground motions. *Earthquake Spectra*, 23(2), 2007, 357-392.
11. Tothong P, Cornell A. Structural performance assessment under near-source pulse-like ground motions using advanced ground motion intensity measures. *Earthquake Engineering & Structural Dynamics*, 37(7), 2008, 1013-1037.
12. Shome N, Cornell C. Normalization and scaling accelerograms for nonlinear structural analysis. *6th U.S. National Conf. on Earthquake Engin*., Seattle, WA, 1998. (CD-ROM)
13. Shome N, Cornell C, Bazzurro P, Carballo J. Earthquakes, records, and nonlinear responses. *Earthquake Spectra*, 14, 1998, 469-500.
14. Cordova P, Deierlein G, Mehanny S, Cornell C. Development of a two parameter seismic intensity measure for probabilistic assessment procedure. Second U.S.-Japan Workshop on Performance-Based Earthquake Engineering Methodology for Reinforced Concrete Building Structures, Sapporo, Japan, 2000, PEER Center, University of California, Berkeley; 195-214.
15. Kurama Y, Farrow K. Ground motion scaling methods for different site conditions and structure characteristics. *Earthquake Engineering & Structural Dynamics*, 32(15), 2003, 2425-2450.
16. Alavi B, Krawinkler H. Behavior of moment-resisting frame structures subjected to near-fault ground motions. *Earthquake Engineering &Structural Dynamics,* 33(6), 2004, 687-706.
17. Bazzurro P, Luco N. Parameterization of non-stationary acceleration time histories. Lifelines Program Project 1G00 Addenda. Pacific Earthquake Engineering Research (PEER) Center, University of California: Berkeley, CA, 2004, 83 pp.
18. Kalkan E, Chopra AK. Practical guidelines to select and scale earthquake records for nonlinear response history analysis of structures. U.S. Geological Survey Open-File Report 2010-1068, 2010, 126.
19. Kalkan E, Chopra AK. Modal-pushover-based ground motion scaling procedure. *J. of Structural Engineering*, 137(3), 2011, 289-310.
20. Kalkan E, Kwong NS. Documentation for assessment of modal pushover-based scaling procedure for nonlinear response history analysis of "ordinary standard" bridges. U.S. Geological Survey Open-File Report 2010-1328, 2011, 58.

For Peer Review

21. Dyke S, Spencer B, Sain M. An experimental study of MR dampers for seismic protection. *Smart Materials & Structures*, 7(5), 1998, 693-703.
22. Mo Y, Lee Y. Shake table tests on small-scale low-rise structural walls with various sections. *Magazine of Concrete Research*, 52(3), 2000, 177-184.
23. Rodriguez M, Restrepo J, Blandon J. Shaking table tests of a four-story miniature steel building - Model validation. *Earthquake Spectra*, 22(3), 2006, 755-780.
24. Lafortune P, McCormick J, DesRoches R. Testing of superelastic recentering pre-strained braces for seismic resistant design. *J. of Earthquake Engineering*, 11(3), 2007, 383-399.
25. ICBO. International Building Code. International Conference of Building Officials, Whittier, CA, 2006.
26. ICBO. California Building Code. International Conference of Building Officials, Whittier, CA, 2007.
27. ASCE. Minimum design loads for buildings and other structures. American Society of Civil Engineers, ASCE Standard No. ASCE/SEI 7-05, Reston, VA, 2006.
28. ASCE. Minimum design loads for buildings and other structures. American Society of Civil Engineers, ASCE Standard No. ASCE/SEI 7-10, Reston, VA, 2010.
29. Reyesm JC, Kalkan E. Required number of records for ASCE/SEI 7 ground motion scaling procedure. U.S. Geological Survey Open-File Report 2011 - 1083, 2011, 34.
30. Anderson J, Bertero VV. Uncertainties in establishing design earthquakes. *J. of Structural Engineering*, 113(8), 1987, 1709-1724.
31. Naeim F, Anderson J. Classification and evaluation of earthquake records for design. CE 93-08, Dept. of Civil Engineering, Univ. of Southern California, Los Angeles, 1993.
32. Naeim F, Anderson J, Jain S. A data base of earthquake records for design. *Fifth U.S. National Conference on Earthquake Engineering*, Oakland, California, 1994, 263-272.
33. Kalkan E, Kunnath SK. Effects of fling-step and forward directivity on the seismic response of buildings. *Earthquake Spectra*, 22(2), 2006, 367-390.
34. Kalkan E, Kunnath SK. Relevance of absolute and relative energy content in seismic evaluation of structures. *Advances in Struc. Eng.*, 11(1), 2008, 17-34.
35. Baker JW. Quantitative classification of near-fault ground motions using wavelet analysis. *Bulletin of the Seismological Society of America*, 97(5), 2007, 1486-1501.
36. PEER Next Generation of Attenuation (NGA) project ground motions database. Pacific Earthquake Engineering Research Center, http://peer.berkeley.edu/products/strong_ground_motion_db.html.
37. Craig RR, Kurdila AJ. Fundamentals of Structural Dynamics. Second Edition, John Wiley and Sons, Inc., 2006, 74-75
38. Mazzoni S, McKenna F, Scott M, Fenves G. Open System for Earthquake Engineering Simulation: OpenSEES command language manual. University of California, Berkeley. (available online at http://opensees.berkeley.edu/)
39. Prakash V, Powell G, Campbell S. DRAIN-2DX base program description and user guide; Version 1.10. University of California, Berkeley, Research Report UCB/SEMM-93/17, 1993.

For Peer Review